Original Article

Influence of sheared edges on the susceptibility to hydrogen embrittlement in third-generation AHSS

Marcus Vinicius Pereira Arruda [1*]
Fernando de Souza Costa [1]
Robson Andrade Paiva [1]
Luiz Fernando Maia de Almeida [2]
Sinésio Domingues Franco [3]

Abstract

Hydrogen embrittlement remains a critical barrier to the effective development and deployment of advanced high-strength steels (AHSS) in automotive applications. The interplay between multiple hydrogen sources and the mechanical stresses inherent to AHSS manufacturing and service conditions contributes to a complex phenomenon that has garnered considerable interest from both industry and academia. In this context, the deformation and defects generated along sheared edges, commonly produced during stamping operations, serve as preferential sites for hydrogen-induced damage, especially delayed cracking. These localized imperfections act as stress concentrators, intensifying the material's susceptibility to embrittlement under hydrogen exposure. This study investigates the combined effect of hydrogen and varying shear cutting conditions on a third-generation AHSS with a tensile strength of 1000 MPa. To this end, specimens electrochemically pre-charged with different hydrogen concentrations and subjected to distinct cutting conditions were evaluated under constant load. The findings quantify the impact of sheared edge quality on the material's susceptibility to hydrogen embrittlement, showing that suboptimal cutting conditions can reduce the critical hydrogen threshold by up to 60% compared to the optimal condition for the steel under study. These results underscore the importance of controlling edge quality during forming operations to mitigate hydrogen-related failures in AHSS components.

Keywords: Advanced high strength steel; Hydrogen embrittlement; Delayed cracking; Sheared edge.

1 Introduction

The susceptibility of advanced high-strength steels (AHSS) to hydrogen embrittlement (HE) remains a critical challenge in the automotive industry, particularly as the demand for steels with increasingly higher strength levels continues to grow. HE typically results from the synergistic interaction between material characteristics, mechanical stresses, both applied and residual, and environmental conditions that facilitate the ingress of diffusible hydrogen into the steel matrix. AHSS, especially those with tensile strengths exceeding 1000 MPa, are particularly vulnerable due to their complex microstructures, often dominated by martensitic phases, which are known to be more prone to hydrogen-induced damage [1,2].

Bergmann et al. [3] highlights that hydrogen content and stress levels fluctuate significantly throughout the lifecycle of an automotive steel component—from steelmaking, through forming operations at the automotive plant, to exposure during vehicle service. Initial hydrogen uptake occurs in the melt shop, influenced by the moisture content of raw materials. While vacuum degassing and reheating prior to hot rolling can reduce metallurgical hydrogen, most of the absorbed hydrogen effuses during solidification due to the sharp decline in solubility at lower temperatures.

Additional hydrogen absorption occurs during pickling with sulfuric or hydrochloric acid, used to remove scale after hot rolling, and within the continuous annealing line. These stages are typically discontinuous due to logistical constraints, allowing for partial hydrogen effusion during intermediate storage [4].

The final and most critical stage in the production of cold-rolled and electrogalvanized AHSS sheets is electrolytic galvanizing. During activation and cleaning, hydrogen is absorbed and subsequently trapped beneath the zinc coating, which significantly impedes its effusion. Depending on the steel grade and process parameters, this step can introduce between 0.1 and 1.0 wppm of hydrogen [3,4]. Similarly, continuous hot-dip galvanizing (CHDG) can result in hydrogen uptake of up to 0.7 wppm, primarily during annealing in H_2-N_2 atmospheres. The extent of absorption is influenced by the furnace atmosphere and the martensitic content of the steel.

[1]*Pesquisa e Desenvolvimento, Usinas Siderúrgicas de Minas Gerais - Usiminas, Ipatinga, MG, Brasil.*
[2]*Laboratório de Tecnologia de Atrito e Desgaste - LTAD, Uberlândia, MG, Brasil.*
[3]*Universidade Federal de Uberlândia, Uberlândia, MG, Brasil.*

[*]*Corresponding author:* marcus.arruda@usiminas.com
E-mails: fernando.costa@usiminas.com; r.paiva@usiminas.com; luiz.almeida@ltad.com.br; sdfranco@ufu.br

An overaging step prior to zinc dipping can reduce the final diffusible hydrogen content to approximately 0.2 wppm [5].

In the body-in-white (BIW) assembly, resistance spot welding (RSW) is widely used for joining structural components. As a thermal joining process, RSW introduces localized microstructural changes and residual stresses, both of which exacerbate HE susceptibility. The formation of hardness gradients and stress concentrations around the weld nugget further intensifies the risk of delayed cracking [6,7].

Following welding, the painting process, particularly phosphating and electro-deposition (e-coating), is another significant source of hydrogen ingress. Cathodic reactions in aqueous environments during these treatments facilitate hydrogen absorption, increasing the potential for embrittlement [8].

The final and least predictable hydrogen uptake occurs during the vehicle's service life, primarily due to corrosion. Although the use of galvanized steel sheets provides long-term corrosion protection, localized damage to the zinc layer or exposed blank edges can form galvanic couples between the steel and zinc. The disparity in surface area between the zinc (anode) and exposed steel (cathode) accelerates hydrogen generation at the cathodic sites, posing a latent risk for HE [6,8].

Regarding stress increases, forming, punching, and welding processes are particularly critical. Furthermore, during vehicle operation, HE may be triggered by hydrogen generated through corrosion processes, especially when combined with static or cyclic mechanical loading (fatigue). Drexler et al. [4] demonstrated that severe plastic deformation in shear-cut edge regions significantly enhances hydrogen's role in delayed crack formation.

In this context, the present study aims to identify critical hydrogen concentrations in combination with varying shear cutting conditions, thereby contributing to the safe application of third-generation AHSS with tensile strengths around 1000 MPa. To achieve this, specimens were precharged with different hydrogen levels and subjected to distinct cutting conditions by varying tool clearance during punching. These samples were then evaluated using constant load tests (CLT) to assess their susceptibility to HE.

2 Development

2.1 Materials and methods

2.1.1 Material

In this study, an industrially uncoated cold-rolled sheet of third-generation transformation-induced plasticity (TRIP) steel, characterized by a nominal tensile strength of 1000 MPa, a thickness of 1.5 mm and a carbon-manganese-silicon (C-Mn-Si) based chemical composition, was evaluated. For hydrogen charging and CLT, which are described in the following sections, test specimens were prepared using electrical discharge machining (EDM), according to the geometry shown in Figure 1. The longitudinal edge of the specimens was oriented perpendicular to the rolling direction. The clamping holes, with a diameter of 8.5 mm, were machined by drilling, and the central hole (10 mm) was punched using different clearance values. The punching procedure is detailed in Section 2.1.3.

Microstructural characterization was performed using scanning electron microscopy (SEM). The samples were prepared following conventional metallographic procedures, including cutting, grinding, and polishing, followed by etching with a 2% Nital solution. To evaluate the amount and distribution of retained austenite, phase maps were obtained via electron backscatter diffraction (EBSD), using an accelerating voltage of 20 kV and a step size of 0.08 μm. Tensile tests were conducted in accordance with ASTM A370 [9], using sheet-type specimens with a gauge length of 50 mm.

2.1.2 Hydrogen charging

To eliminate any residual hydrogen content, the test specimens were subjected to a thermal desorption treatment

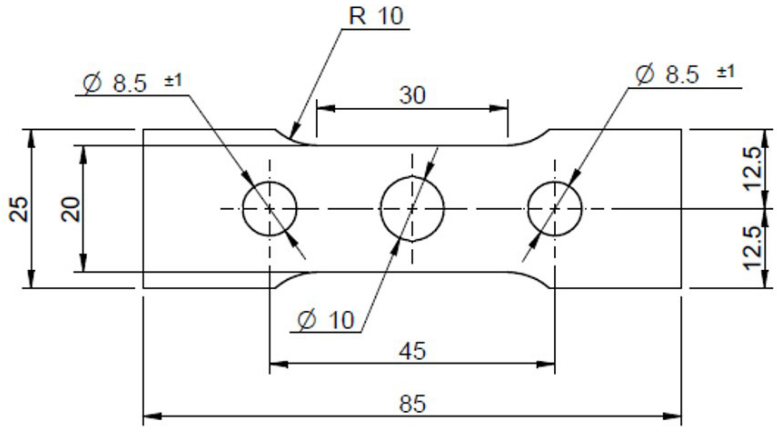

Figure 1. Geometry of the test specimen used during ex-situ charging and CLT.

(baking), which involved heating in a muffle furnace to 100 °C and maintaining this temperature for 24 hours. To ensure uniform surface conditions, all samples were ground prior to hydrogen charging using silicon carbide abrasive pads with grit sizes of 220 and 600. Cathodic charging was carried out in an electrochemical cell, where the sample served as the working electrode and platinum core was used as the inert anode.

The electrolyte consisted of a 0.1 M NaOH solution with varying concentrations of ammonium thiocyanate (NH_4SCN) to adjust the hydrogen content, as detailed in Table 1. The schematic of the electrochemical cell setup is shown in Figure 2.

Immediately after hydrogen charging, the test specimens were electrochemically coated with zinc to minimize hydrogen effusion during the CLT. For this purpose, the specimens were mounted in an electrochemical cell equipped with an inert iridium anode, and a constant current density of 20 mA/cm^2 was applied for 20 seconds. The electrolyte solution consisted of 100 g of Zn^{2+} and 5 g of H_2SO_4 dissolved in one liter of distilled water.

Hydrogen quantification in the test specimens was performed by hot extraction using a G8 GALILEO analyzer equipped with a thermal conductivity detector (TCD), offering a resolution of 0.01 ppm. For detector calibration, a standard gas mixture containing 5 ppm of H_2 in high-purity helium was used, with nitrogen (N_2 5.0) serving as the carrier gas. The analysis was conducted under isothermal conditions at 350 °C for 45 minutes. For each evaluated charging condition, three hydrogen content measurements were performed. The defined hydrogen concentrations for each permeation condition were subsequently reproduced during the charging of specimens used in the CLT.

2.1.3 Constant Load Testing - CLT

The critical hydrogen content associated with different sheared edge conditions was determined through CLT, using the pre-charged specimens described in the previous section.

The severity of deformation at the edge of the punched central hole was assessed by varying the cutting clearances in conical hole expansion tests (HET).

These tests were performed in accordance with ISO 16630 standard [10], which defines the calculation of the hole expansion ratio ($HER_{\%}$) according to Equation 1. For each clearance condition, the average $HER_{\%}$ was calculated from the results of three test specimens.

$$HER_{\%} = \left(Df - Di\right) / Di \times 100 \quad (1)$$

Where:
Di: initial hole diameter (10 mm);
Df: final hole diameter.

With the cutting clearances defined, the die/punch set was mounted on an interchangeable punching device coupled to a hydraulic press. After hole punching, the specimens were mounted on proof ring loading devices, applying a stress equivalent to 100% of the yield strength of the evaluated steel. The proof rings, originally designed for stress corrosion testing (SCT), were adapted for flat specimen testing in accordance with SEP1970 standard [11]. The testing force was generated by the spring-back of the compressed ring

Table 1. Electrochemical conditions used for ex-situ cathodic hydrogen charging

Conditions	Current (mA/cm²)	Time (min)	NH_4SCN (g/L)
1	10	60	0
2			1
3			3

(a) (b)

Figure 2. (a) Test setup and (b) beaker glass detail used for electrochemical hydrogen charging.

and calculated by multiplying measured diameter reduction by the spring constant of each individual ring. The spring constant was measured and calibrated using a load cell. The applied stress on the specimen was determined by dividing the testing force by the remaining cross-sectional area. The desired testing force was adjusted by compressing the ring with a screw, while the corresponding diameter reduction was measured using a digital vernier caliper, with a nominal range of 300 mm and an accuracy of 0.01 mm. Figures 3 and 4 illustrate the punching sequence and the test setup for the specimens mounted on the rings, respectively. To prevent hydrogen effusion, the entire operation, from punching to specimen assembly on the rings, was completed within the 10-minute limit recommended by SEP1970 [11].

To identify possible changes in the failure mode associated with hydrogen embrittlement, the fracture surfaces of the failed test specimens were examined using scanning electron microscopy (SEM). Additionally, Vickers microhardness (HV0.05) maps were generated on cross-sections of the punched edges, extending up to 1 mm from the edge surface.

2.2 Results and discussion

2.2.1 Initial characterization

As shown in Figure 5, the microstructure observed by SEM revealed the typical constituents of TRIP steel, including fractions of ferrite (α), bainite (γB), martensite (γM), and retained austenite (RA). The volume fraction of retained austenite (FCC), measured by electron backscatter diffraction (EBSD), was approximately 15%.

The main mechanical properties obtained from tensile and hole expansion tests on the as-received samples are summarized in Table 2. As expected, the measured values are consistent with those typically reported for TRIP steels, which are characterized by a high strain-hardening capacity due to the presence of retained austenite in their microstructure. Figure 6a presents the engineering stress–strain curve obtained from tensile tests on uncharged samples. The edge stretchability, evaluated through the hole expansion test under different cutting clearances (Figure 6b), reached its maximum at a 12%t clearance, while the lowest value was observed at 25%t. Based on these results, the 12%t and

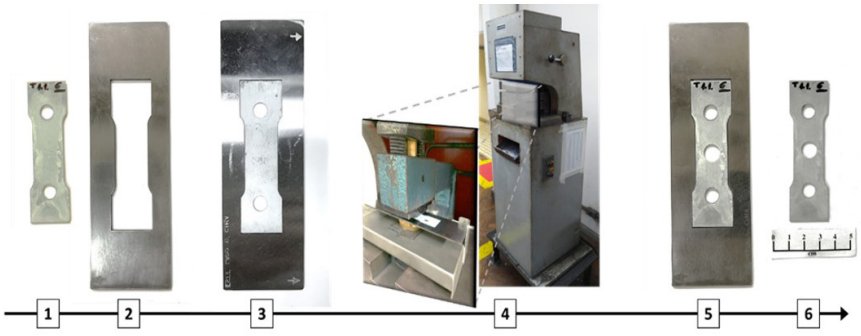

1 – Precharged test specimen
2 – Hole positioning fixture
3 – Assembly the specimen on hole positioning
4 – Specimen assembly positioned for forming in the hydraulic press
5 – Specimen assembly after punching
6 – Specimen ready for mounting on the proof ring

Figure 3. Sequence of steps for making the punched central hole of the specimens intended for CLT.

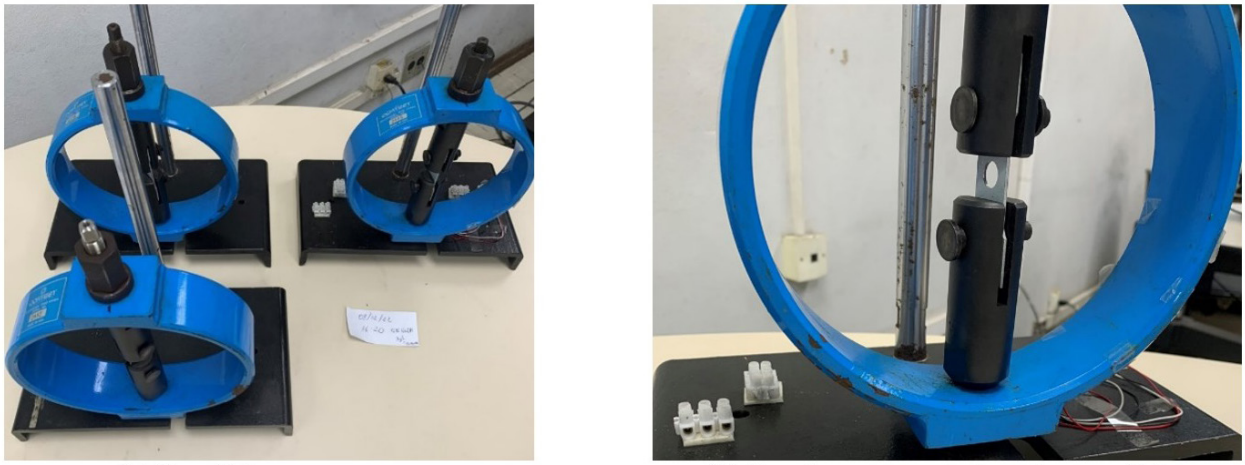

(a) Proof rings (b) Specimen mounted on the proof ring

Figure 4. Scheme for assembly the test specimens on proof rings after hydrogen permeation and punching.

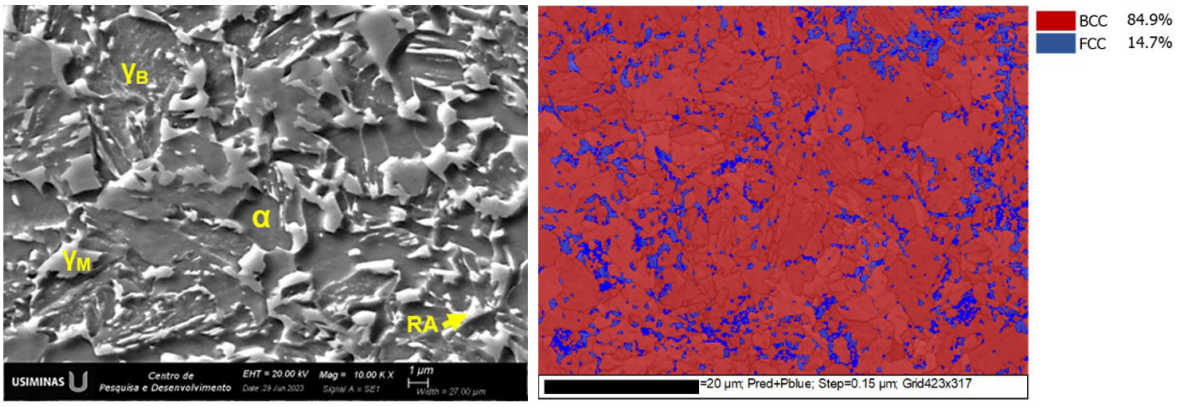

Figure 5. (a) SEM micrograph and (b) phase map by EBSD of the TRIP steel class.

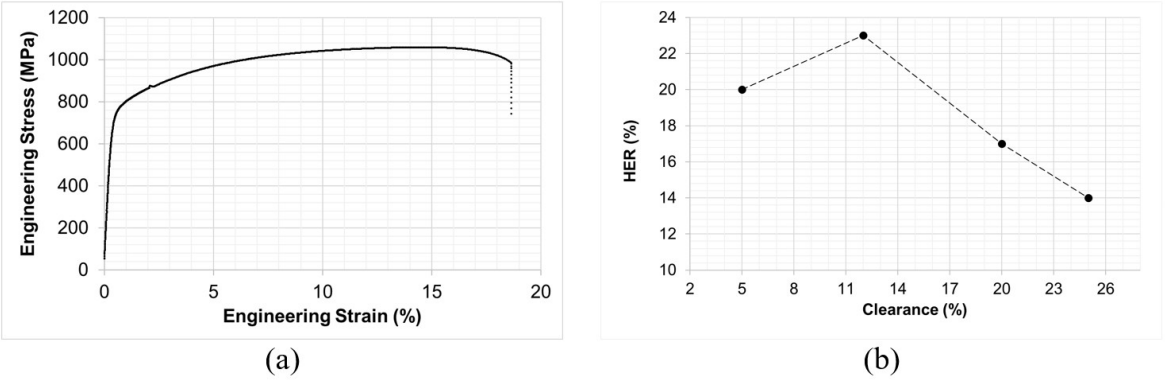

Figure 6. (a) Typical stress–strain curve of the steel; (b) Hole Expansion Ratio (HER) results for different cutting clearances.

Table 2. Mechanical properties in the as-received conditions

YS (MPa)	UTS (MPa)	EL (%)	Shearing clearance		HER (%)
			(%t)	(mm)	
758	1067	19	5	0.075	20
			12	0.175	23
			20	0.30	17
			25	0.40	14

25%t clearances were selected as distinct cutting conditions for comparison in the hydrogen embrittlement tests.

The cross-sectional and surface images of the sheared edges, along with the microhardness maps and profiles, were analyzed based on the rollover, burnishing, and fracture zones to assess the effect of shear clearance on the degree of hardening in each region.

As shown in Figure 7, the size of the rollover zone increased considerably with cutting clearance, while the shear zone exhibited a slight reduction. In contrast, the extent of the fracture zone did not change significantly. However, a noticeable increase in the fracture angle was observed. According to the hardness maps, the depth of the shear-affected zone was greater for the 25%t cutting clearance.

The microhardness profile results indicate that, with increasing clearance, the maximum microhardness values increased from 373 HV to 397 HV in the rollover zone, from 468 HV to 469 HV in the burnishing zone, and from 453 HV to 486 HV in the fracture zone, corresponding to clearances of 12%t and 25%t, respectively. In other words, the rollover and fracture zones exhibited an increase in hardness. These results indicate a higher degree of hardening at the sheared edge as the clearance increased from 12%t to 25%t.

Severe localized plastic deformation induces pre-damage in the shear-affected zone of punched edges, compromising the flange stretchability of AHSS, as measured, for instance, by hole expansion tests. This deformation also increases the dislocation density and the number of crystalline defects,

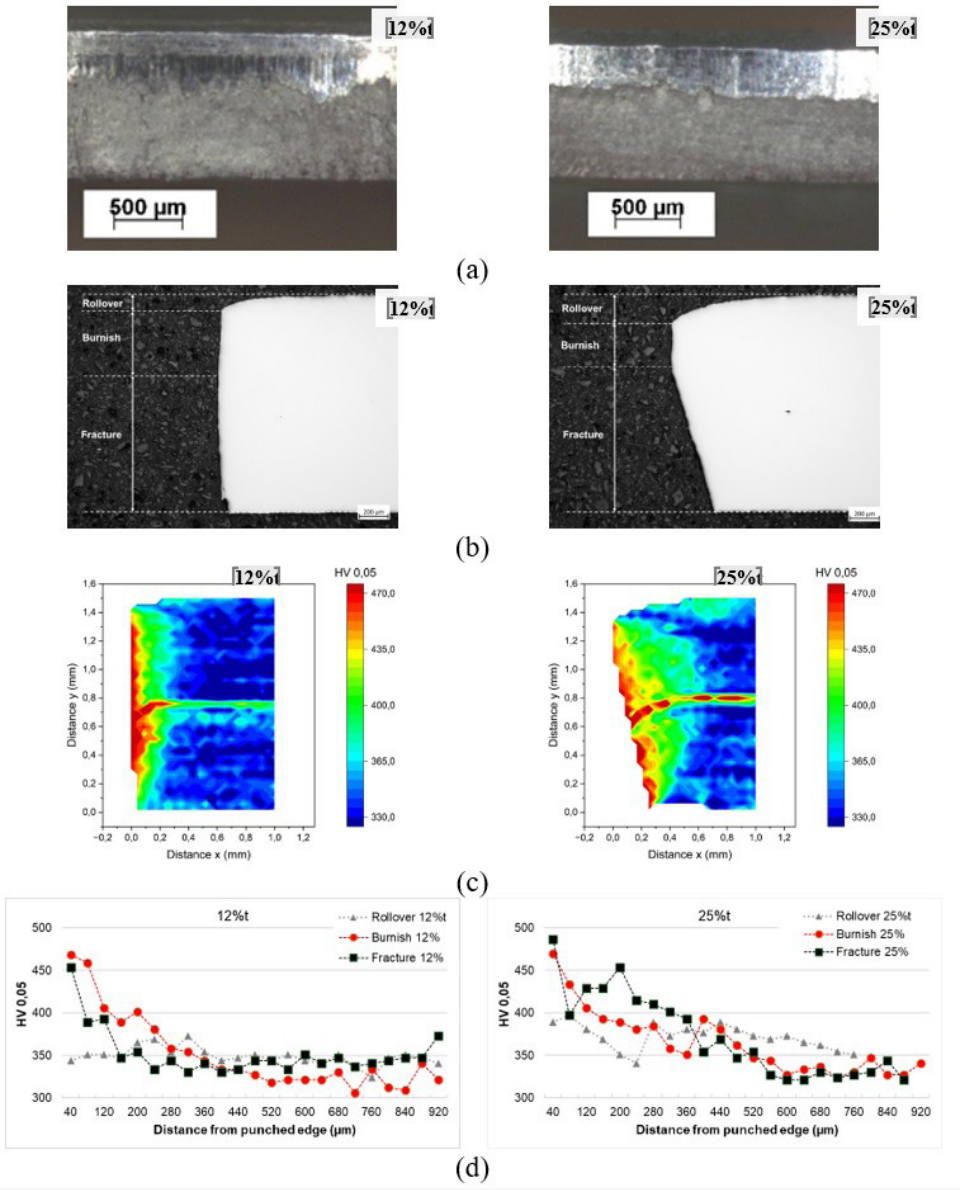

Figure 7. Images of sheared edges under different clearances. (a) Cross-sectional images; (b) Surface images; (c) Microhardness map and (d) Microhardness profiles of sheared edge in Rollover, Burnish and Fracture zones.

which are known to act as hydrogen traps. Consequently, local hydrogen accumulation occurs, as reported by Drexler et al. [4] and Ozdirik et al. [12].

2.2.2 Electrochemical charging

Figure 8 presents the average hydrogen content (ppm) obtained under different electrochemical charging conditions. The results indicate that the baking treatment was effective in eliminating any residual hydrogen. Increasing the concentration of ammonium thiocyanate led to progressively higher hydrogen levels, with average values of 0.24 ppm, 0.61 ppm, and 0.87 ppm corresponding to concentrations of 0 g/L, 1 g/L, and 3 g/L, respectively. Notably, according to the literature, the diffusible hydrogen content measured after various stages of industrial processing of AHSS, whether at the steel mill or during automotive manufacturing, is typically below or close to 1 ppm [3,4]. Therefore, the charging conditions employed in this study resulted in hydrogen levels consistent with those encountered in industrial practice.

2.2.3 Critical hydrogen determination in CLT

The results of the CLT for pre-loaded samples are shown in Figure 9. Each empty red circle in the diagram represents a sample that failed within 100 hours for a given hydrogen concentration. The filled green circle indicates a non-failure condition, where the sample remained intact and free of cracks for more than 100 hours.

In these diagrams, the critical hydrogen content (CH) is defined as the highest hydrogen concentration at which none of the three samples failed after 100 hours of testing. This evaluation revealed CH values of 0.61 ppm and 0.24 ppm for cutting clearances of 12%t and 25%t, respectively. These results demonstrate that an inadequate cutting condition, specifically the excessive clearance of 25%t, reduced the critical hydrogen content by 60% compared to the optimal clearance of 12%t for this steel.

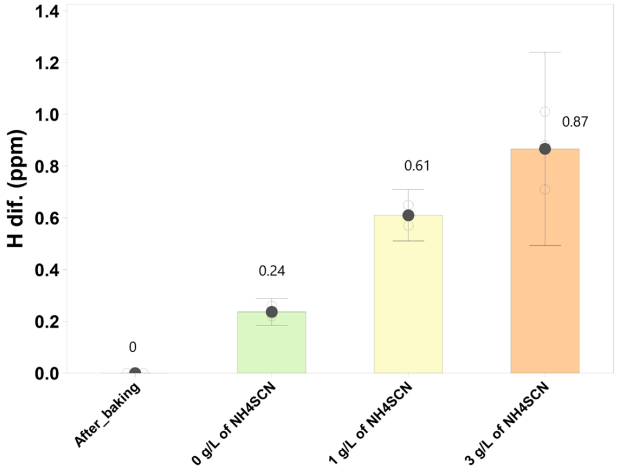

Figure 8. Average diffusible hydrogen content after electrochemical charging.

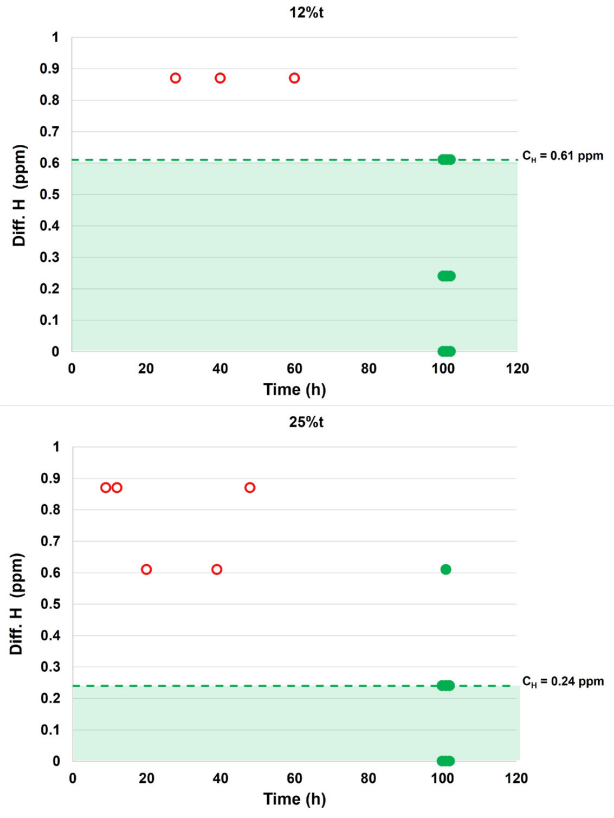

Figure 9. Results of CLT in samples with punched holes of (a) 12% and (b) 25% cutting clearance.

The increased susceptibility to delayed cracking observed at the 25% clearance can be explained by the larger shear-affected zone, which is characterized by severe plastic deformation and a high density of microstructural defects, key factors for localized hydrogen accumulation.

Additionally, the significant presence of retained austenite in the microstructure of TRIP steels may enhance this effect. Due to its compact face-centered cubic (FCC) crystal structure, retained austenite exhibits a low hydrogen diffusion coefficient and a high hydrogen solubility compared to other phases present in AHSS. As a result, this phase can act as a hydrogen container, reducing hydrogen concentration in critical regions such as crack tips, thereby delaying material embrittlement [13].

However, during localized deformation in the shear-affected zone, hydrogen trapped in retained austenite tends to be released into the lattice when this phase transforms into martensite through the TRIP effect during plastic deformation, which can have a highly detrimental effect on the ductility of these steels [14].

2.2.4 Fractography

Figure 10 shows the fracture surfaces of specimens that failed during CLT conducted with a 25%t clearance under two different hydrogen charging conditions. In all cases, fracture initiation occurred at the punched shear edge, confirming that the central hole acted as an effective stress concentrator.

The fracture surfaces exhibited a predominantly brittle morphology originating at the sheared edge and propagating toward the mid-thickness of the material.

As the hydrogen content increased, the fracture surface in the central propagation region became more brittle. It transitioned from a mixed-mode fracture characterized by ductile features such as microvoid coalescence (dimples) alongside cleavage facets (Figure 10c), to a predominantly brittle, transgranular cleavage fracture, with some open grain boundaries indicative of intergranular failure. This transition is consistent with typical hydrogen-induced fracture mechanisms observed in AHSS.

Another effect of elevated hydrogen content was the substantial expansion of the brittle region at mid-thickness. This behavior may be explained by Beachem's theory [15], which correlates fracture morphology with local hydrogen concentration and the presence of martensite formed from retained austenite via TRIP effect.

Surrounding the brittle zone, a lighter region on the fracture surface, corresponding to the final fracture or burst zone, displayed a predominantly ductile morphology, characterized by microvoid coalescence.

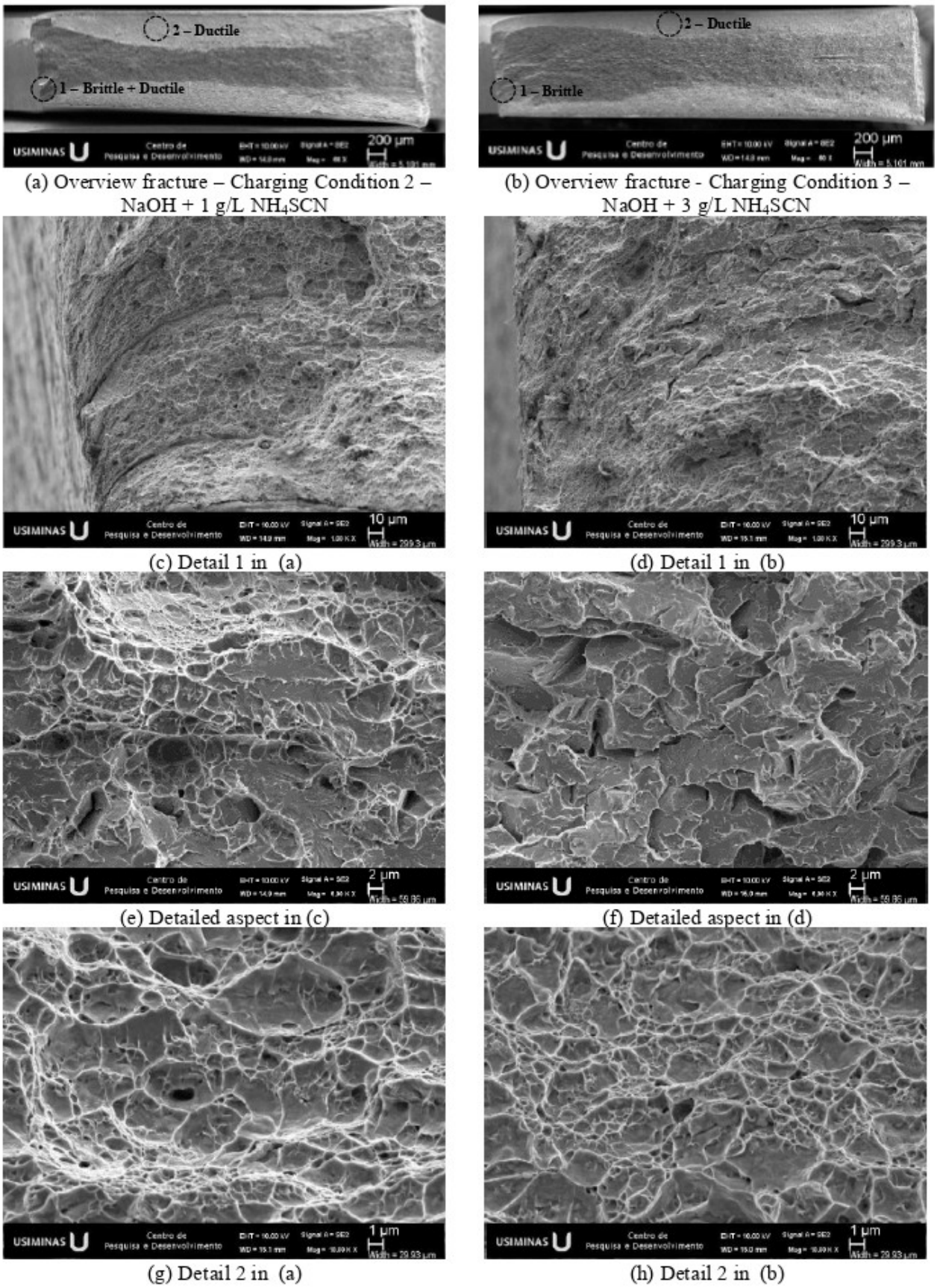

(a) Overview fracture – Charging Condition 2 – NaOH + 1 g/L NH_4SCN

(b) Overview fracture - Charging Condition 3 – NaOH + 3 g/L NH_4SCN

(c) Detail 1 in (a)

(d) Detail 1 in (b)

(e) Detailed aspect in (c)

(f) Detailed aspect in (d)

(g) Detail 2 in (a)

(h) Detail 2 in (b)

Figure 10. Different regions of the fracture surfaces of CLT specimens tested with 25% cutting clearance, precharged under hydrogen charging conditions 2 (NaOH + 1 g/L NH_4SCN) and 3 (NaOH + 3 g/L NH_4SCN).

3 Conclusions

The influence of shearing edge condition on the hydrogen-induced delayed cracking susceptibility of a third-generation AHSS was investigated through microstructural characterization, microhardness measurements, and constant load testing.

The sheared edge surface was found to be hardened due to strain hardening and the transformation of metastable austenite into martensite via TRIP effect. With increasing cutting clearance, both the depth and intensity of hardening at the sheared edge increased, reducing formability. Furthermore, the hardness uniformity of the hardened layer decreases as clearance increased, leading to localized variations in microhardness that promote crack initiation.

CLT on specimens precharged with different hydrogen contents and subjected to varying cutting clearances demonstrated that an inadequate edge quality, characterized by excessive clearance, reduced the critical hydrogen content by 60% compared to the optimal cutting condition of 12% of the material thickness.

These findings provide valuable insights for mitigating edge cracking during manufacturing and improved engineering of AHSS components, particularly in the automotive applications.

References

1 Robertson IM, Sofronis P, Nagao A, Martin ML, Wang S, Gross DW, et al. Hydrogen embrittlement understood. Metallurgical and Materials Transactions. B, Process Metallurgy and Materials Processing Science. 2015;46(3):1085-1103. https://doi.org/10.1007/s11663-015-0325-y.

2 Gong P, Turk A, Nutter J, Yu F, Wynne B, Rivera-Diaz-del-Castillo P, et al. Hydrogen embrittlement mechanisms in advanced high strength steel. Acta Materialia. 2022;223:117488. https://doi.org/10.1016/j.actamat.2021.117488.

3 Bergmann C. Hydrogen embrittlement resistance of advanced high strength steel grades in automotive applications [thesis]. Bochum: Ruhr-Universität Bochum; 2020. https://doi.org/10.13154/294-7526.

4 Drexler A, Bergmann C, Manke G, Kokotin V, Mraczek K, Pohl Ecker M. On the local evaluation of the hydrogen susceptibility of cold-formed and heat treated advanced high strength steel (AHSS) sheets. Materials Science and Engineering A. 2021;819:140276. https://doi.org/10.1016/j.msea.2020.140276.

5 Choi DW, Yoo J, Lee JJ, Kim C-W, Lee C-H, Jung S-P, et al. Investigation of mechanism of hydrogen embrittlement susceptibility in resistance spot-welded advanced high-strength steels. Metals and Materials International. 2025. https://doi.org/10.1007/s12540-025-01977-w.

6 Robertson IM, Sofronis P, Nagao A, Martin ML, Wang S, Gross DW, et al. Hydrogen embrittlement understood. Metallurgical and Materials Transactions. B, Process Metallurgy and Materials Processing Science. 2015;46(3):1085-1103. https://doi.org/10.1007/s11663-015-0325-y.

7 Rejeesh R, Jang Y, Park Y-D. Hydrogen embrittlement in resistance spot and laser welds for advanced high-strength steels: mechanisms, susceptibility, and evaluation. Journal of Welding and Joining. 2025;43(3):280-299. https://doi.org/10.5781/JWJ.2025.43.3.7.

8 Ma, MT., Li, KJ., Si, Y, Cao PJ, Lu HZ, Guo AM, et al. Hydrogen embrittlement of advanced high-strength steel for automobile application: a review. Acta Metallurgica Sinica (English Letters). 2023;36:1144-1158. https://doi.org/10.1007/s40195-022-01517-0.

9 American Society for Testing and Materials. ASTM A370 – Standard Test Methods and Definitions for Mechanical Testing of Steel Products. West Conshohocken: ASTM; 2011.

10 International Organization for Standardization. ISO 16630: Metallic materials – Method of hole expanding test. Geneva: ISO; 2003.

11 SEP1970 STAHLINSTITUTS VDEH. 2011-05: Test of the resistance of Advanced High Strength Steels (AHSS) for automotive applications against production related hydrogen induced brittle fracture. Düsseldorf: Stahlinstitut VDEh; 2011.

12 Ozdirik B, Suter T, Hans U, Depover T, Verbeken K, Schmutz P, et al. Study of the hydrogen uptake in deformed steel using the microcapillary cell technique. Corrosion Science. 2019;155:55-66. https://doi.org/10.1016/j.corsci.2019.04.029.

13 Depover T, Wallaert E, Verbeken K. Fractographic analysis of the role of hydrogen diffusion on the hydrogen embrittlement susceptibility of DP steel. Materials Science and Engineering A. 2016;649:111-118. https://doi.org/10.1016/j.msea.2015.09.124.

14 Dwivedi SK, Vishwakarma M. Effect of hydrogen in advanced high strength steel materials. International Journal of Hydrogen Energy. 2019;44(49):26935-26944. https://doi.org/10.1016/j.ijhydene.2019.08.149.

15 Beachem CD. A new model for hydrogen-assisted cracking hydrogen “embrittlement”. Metallurgical Transactions. 1972;3(2):441-455. https://doi.org/10.1007/BF02642048.

Received: 21 Aug 2025
Accepted: 1 Dec 2025

Editor-in-charge:
Paula Fernanda da Silva Farina